RESEARCH ARTICLE SUMMARY

PLANT SCIENCE

Reconstitution and structure of a plant NLR resistosome conferring immunity

Jizong Wang*, Meijuan Hu*, Jia Wang*, Jinfeng Qi, Zhifu Han, Guoxun Wang, Yijun Qi, Hong-Wei Wang†, Jian-Min Zhou†, Jijie Chai†

INTRODUCTION: Nucleotide-binding (NB), leucine-rich repeat (LRR) receptors (NLRs) mediate plant immunity by directly or indirectly sensing pathogen effector proteins delivered into plant cells. The activation of plant NLRs stops pathogen proliferation through the induction of a variety of defenses, including the hypersensitive response, a form of programmed cell death. In the small mustard plant *Arabidopsis thaliana*, the coiled-coil (CC)–NLR HOPZ-ACTIVATED RESISTANCE 1 (ZAR1) exists in a preformed complex with resistance-related kinase 1 (RKS1) to sense the uridylyltransferase effector AvrAC from the microbial pathogen *Xanthomonas campestris* pv. *campestris* (*Xcc*). AvrAC uridylates the PBS1-like protein 2 (PBL2) kinase to produce PBL2^{UMP}, which is recruited to ZAR1-RKS1. As members of the adenosine triphosphatases associated with diverse cellular activities, NLRs are hypothesized to function through oligomerization. Evidence for this model is provided by studies of animal NLRs. However, whether plant NLRs oligomerize after activation into large protein complexes like NLR inflammasomes remains unknown. Furthermore, little is known about the biochemical functions of plant NLRs.

RATIONALE: In an accompanying paper, we show that the ZAR1-RKS1-PBL2^{UMP} complex in the absence of deoxyadenosine triphosphate (dATP) or adenosine triphosphate (ATP) is in a primed state. Gel filtration and cryo–electron microscopy (cryo-EM) were used to investigate whether the primed complex oligomerizes in the presence of dATP or ATP. We verified the biological relevance of the oligomerized ZAR1-RKS1-PBL2^{UMP} complex induced by dATP or ATP with biochemical, cell-based, and functional assays.

RESULTS: Gel filtration analysis showed that ZAR1-RKS1 and PBL2^{UMP} formed a high-order oligomeric complex with a molecular mass of ~900 kDa in the presence of dATP or ATP. We termed the complex the ZAR1 resistosome. A cryo-EM structure of the ZAR1 resistosome determined at a resolution of 3.4 Å revealed that it formed a wheel-like pentamer, the assembly of which is mediated by ZAR1. All the structural domains of ZAR1, including the CC domain, NB domain (NBD), helical domain 1 (HD1), winged-helix domain (WHD), and LRR domain, are involved in the pentamerization of the ZAR1 resistosome, which is further stabilized by dATP. Mutagenesis analyses and functional studies indicate that the resistosome activates the defensive hypersensitive cell death response and contributes to resistance to *Xcc*.

ON OUR WEBSITE

Read the full article at http://dx.doi.org/10.1126/science.aav5870

The ZAR1 CC domain (ZAR1^{CC}) contributes to the oligomerization of the ZAR1 resistosome by forming an α-helical barrel. ZAR1^{CC} undergoes fold switching during ZAR1 activation, in addition to the structural remodeling of ZAR1^{WHD}-ZAR1^{LRR} relative to ZAR1^{NBD}-ZAR1^{HD1}. The very N-terminal α helix (α1) buried in the inactive ZAR1 becomes exposed in the ZAR1 resistosome. The five exposed α1 helices in the ZAR1 resistosome form a funnel-shaped structure projecting out of the wheel-defined plane. Biochemical and functional data showed that this structure is required for AvrAC-induced ZAR1 plasma membrane (PM) association, cell death, and resistance to *Xcc*. Simultaneous mutation of two negatively charged residues at its inner surface did not affect ZAR1 binding to the PM but did abolish cell death and disease resistance, suggesting that the ZAR1 resistosome function requires the inner surface of the funnel structure.

CONCLUSION: Our study revealed the oligomerization of ZAR1, a plant NLR protein; clarified its activation mechanism; and provided insights into its biochemical functions. ■

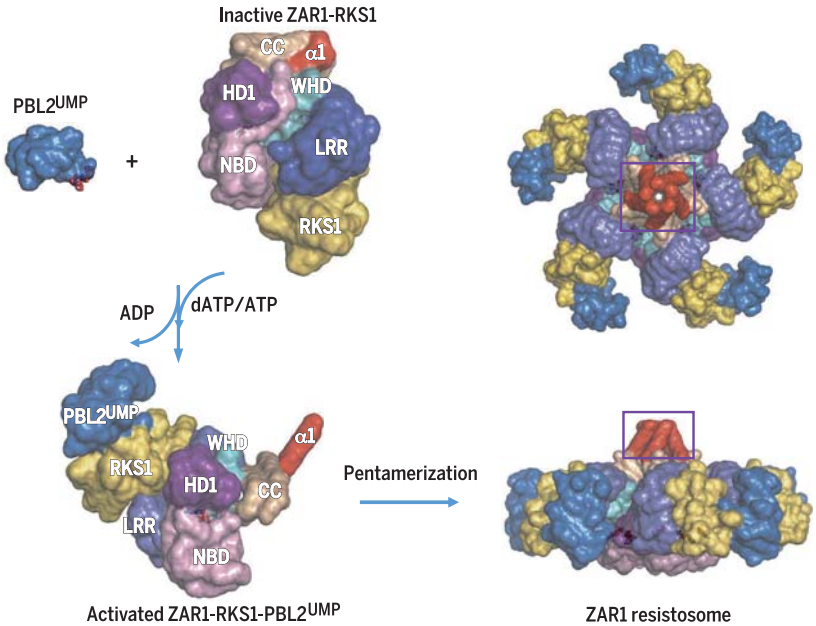

PBL2^{UMP}-induced assembly of the ZAR1 resistosome. Interaction of PBL2^{UMP} (blue) with the preformed ZAR1-RKS1 complex (inactive ZAR1-RKS1) triggers conformational changes in ZAR1^{NBD} and adenosine diphosphate (ADP) release, allowing the complex to bind dATP or ATP. dATP or ATP binding induces structural remodeling and fold switching of ZAR1, resulting in full activation of ZAR1 (activated ZAR1-RKS1-PBL2^{UMP}) and formation of the pentameric ZAR1 resistosome (shown in two orientations). The very N-terminal α helix (α1) (red) of ZAR1 buried in the inactive ZAR1-RKS1 complex becomes solvent-exposed in the activated ZAR1-RKS1-PBL2^{UMP} complex and forms a funnel-shaped structure (highlighted within the purple frame) in the ZAR1 resistosome that is required for ZAR1 PM association, cell death triggering, and disease resistance.

*These authors contributed equally to this work.
The list of author affiliations is available in the full article online.
†Corresponding author. Email: chaijj@tsinghua.edu.cn (J.C.); jmzhou@genetics.ac.cn (J.-M.Z.); hongweiwang@tsinghua.edu.cn (H.-W.W.)
Cite this article as J. Wang *et al.*, *Science* **364**, eaav5870 (2019). DOI: 10.1126/science.aav5870

RESEARCH ARTICLE

PLANT SCIENCE

Reconstitution and structure of a plant NLR resistosome conferring immunity

Jizong Wang[1]*, Meijuan Hu[2]*, Jia Wang[1]*, Jinfeng Qi[2], Zhifu Han[1], Guoxun Wang[2], Yijun Qi[1], Hong-Wei Wang[1]†, Jian-Min Zhou[2]†, Jijie Chai[1,3,4]†

Nucleotide-binding, leucine-rich repeat receptors (NLRs) perceive pathogen effectors to trigger plant immunity. Biochemical mechanisms underlying plant NLR activation have until now remained poorly understood. We reconstituted an active complex containing the *Arabidopsis* coiled-coil NLR ZAR1, the pseudokinase RKS1, uridylated protein kinase PBL2, and 2′-deoxyadenosine 5′-triphosphate (dATP), demonstrating the oligomerization of the complex during immune activation. The cryo–electron microscopy structure reveals a wheel-like pentameric ZAR1 resistosome. Besides the nucleotide-binding domain, the coiled-coil domain of ZAR1 also contributes to resistosome pentamerization by forming an α-helical barrel that interacts with the leucine-rich repeat and winged-helix domains. Structural remodeling and fold switching during activation release the very N-terminal amphipathic α helix of ZAR1 to form a funnel-shaped structure that is required for the plasma membrane association, cell death triggering, and disease resistance, offering clues to the biochemical function of a plant resistosome.

The nucleotide-binding domain (NBD) and leucine-rich repeat (LRR) receptors (NLRs) are a large family of intracellular immune receptors in both animals and plants (*1*, *2*). Unlike animal NLRs that recognize conserved pathogen-associated molecular patterns (*3*, *4*), however, NLRs in plants directly or indirectly mediate immune sensing of typically isolate-specific pathogen effector proteins delivered into plant cells (*5*, *6*). The activation of plant NLRs terminates pathogen proliferation through the induction of an array of immune responses and is often accompanied by a form of localized cell death called the hypersensitive response (HR) (*7*, *8*).

NLR proteins are members of signal transduction adenosine triphosphatases (ATPases) with numerous domains (STANDs) and share a conserved tripartite domain structure consisting of a nonconserved N-terminal domain, a central nucleotide-binding (NB) and oligomerization domain, and a C-terminal LRR domain (*9*). The central conserved region of plant NLRs is also called the NB-ARC domain because of its presence in the founding members Apaf-1, resistance (R) proteins, and CED-4 (*1*, *2*, *5*). Like other STAND ATPases, NLRs are believed to function as molecular switches, with an adenosine 5′-diphosphate (ADP)–bound inactive state and an adenosine 5′-triphosphate (ATP)–bound active state, as supported by studies of Apaf-1 (*10*, *11*), animal NLRs (*12*, *13*), and several plant NLRs (*14*–*16*). Once activated, Apaf-1 and some animal NLRs oligomerize into apoptosomes (*17*) and inflammasomes (*18*–*20*), respectively, both of which function as caspase-activating platforms (*21*, *22*). Our structural and biochemical understanding of plant NLR activation is much less complete (*23*) than that of Apaf-1 and animal NLRs. Whether and how activated plant NLRs oligomerize into large protein complexes such as apoptosomes and inflammasomes remain unclear. Although components immediately downstream of plant NLR signaling remain undefined, the N-terminal coiled-coil (CC) domain and Toll/interleukin-1 receptor (TIR) domain likely function as signaling modules in plant NLR proteins, because their overexpression in plants is sufficient to induce the activation of HR cell death and disease resistance in several cases (*24*–*28*). However, whether the CC and TIR domains of plant NLRs are functionally analogous to the N-terminal caspase activation and recruitment domains (CARDs) of animal NLRs (*21*) or Apaf-1 (*22*) and act as scaffolds for signal transduction is unknown.

ZAR1 (HOPZ-ACTIVATED RESISTANCE 1), a canonical CC-NLR protein shared by *Arabidopsis* (*29*) and *Nicotiana benthamiana* (*30*), is organized into distinct preformed immune receptor complexes by interacting with multiple members of the subfamily XII-2 receptor–like cytoplasmic kinases (RLCKs), and each preformed immune receptor complex detects a specific bacterial effector to trigger effector-triggered immunity (*31*–*33*). We previously showed that one such complex, ZAR1–RKS1 (resistance-related kinase 1), confers resistance to disease caused by *Xanthomonas campestris* bacteria carrying the effector protein AvrAC, an enzyme that uridylylates multiple members of the RLCK VII subfamily. One of these AvrAC-modified proteins, PBL2 [with the modified form designated PBL2^{UMP} to indicate the transfer of uridine monophosphate (UMP) by uridylylation], is specifically recognized as a ligand by the preformed ZAR1-RKS1 complex and consequently triggers ZAR1-mediated immunity (*32*). In the accompanying paper (*34*), we show that the recruitment of PBL2^{UMP} to ZAR1-RKS1 allosterically facilitates the release of ADP from ZAR1, leading to a primed state of the ZAR1-RKS1-PBL2^{UMP} complex that may be readily activated by incorporating dATP or ATP into ZAR1.

Whereas studies of the animal NLR family apoptosis inhibitory protein (NAIP)–NLRC4 pairs (*13*, *18*–*20*, *35*), Apaf-1 (*10*, *11*, *17*), and CED-4 have shown oligomerization as a central mechanism in the activation of these proteins (*36*), whether similar mechanisms apply to plant NLR activation remains unknown. In the present study, we reconstituted in vitro an oligomeric ZAR1-RKS1-PBL2^{UMP} complex, which we term the ZAR1 resistosome. Cryo–electron microscopy (cryo-EM) reveals a wheel-like pentameric structure at a 3.4-Å resolution for the ZAR1 resistosome, reminiscent of those of the NLRC4 inflammasome (*18*–*20*) and Apaf-1 apoptosome (*17*). However, in contrast with the disordered CARDs in the latter two large protein complexes, the oligomeric CC domains in the ZAR1 resistosome form an α-helical barrel structure, the bulk of which is buried through interaction with the oligomerized LRR and winged-helix domains. Structural comparison shows that the CC domain undergoes fold switching during activation, in addition to the structural reorganization between the winged-helix domain (WHD) and helical domain 1 (HD1). These structural changes result in the release of the very N-terminal amphipathic α helix of ZAR1. The released α helices in the ZAR1 resistosome are solvent exposed and form a funnel-shaped structure. Functional data indicate that this structure is essential for the immune signaling and membrane-association activities of ZAR1. Taken together, our data reveal the assembly mechanism of an active plant NLR complex and suggest different signaling mechanisms between plant and animal NLRs.

Results

Reconstitution and cryo-EM reconstruction of the ZAR1 resistosome

The accompanying study (*34*) showed that the binding of PBL2^{UMP} to the preformed ZAR1-RKS1

[1]Beijing Advanced Innovation Center for Structural Biology, Tsinghua-Peking Joint Center for Life Sciences, Center for Plant Biology, School of Life Sciences, Tsinghua University, 100084 Beijing, China. [2]State Key Laboratory of Plant Genomics, Institute of Genetics and Developmental Biology, Academy of Seed Design, Chinese Academy of Sciences, 100101 Beijing, China. [3]Max Planck Institute for Plant Breeding Research, Cologne, Germany. [4]Institute of Biochemistry, University of Cologne, Zuelpicher Strasse 47, 50674 Cologne, Germany.
*These authors contributed equally to this work.
†Corresponding author. Email: chaijj@tsinghua.edu.cn (J.C.); jmzhou@genetics.ac.cn (J.-M.Z.); hongweiwang@tsinghua.edu.cn (H.-W.W.)

complex promotes ADP release from ZAR1, forming an intermediate complex containing ZAR1, RKS1, and PBL2^{UMP}. To test whether a nucleoside triphosphate binds the intermediate state of ZAR1 and consequently induces its oligomerization, the ZAR1-RKS1 complex and PBL2^{UMP} proteins purified as previously described were incubated with ATP or dATP and then subjected to gel filtration analysis. As shown in Fig. 1A and fig. S1A, incubation with 1.0 mM dATP or ATP shifted the protein complex containing ZAR1, RKS1, and PBL2^{UMP} but not ZAR1-RKS1 alone (fig. S1B) or ZAR1-RKS1 with PBL2 (fig. S1C) to a higher-molecular-mass species with a molecular mass of ~900 kDa, indicating that dATP or ATP induced oligomerization of the tertiary complex. We term the dATP- or ATP-induced oligomer the ZAR1 resistosome. dATP appeared to be more active than ATP in inducing the formation of the ZAR1 resistosome (Fig. 1A and fig. S1A), as observed in the assembly of the Apaf-1 apoptosome (*37*), but the biological roles of this distinction remain unclear. By contrast, the same concentration of ADP had no activity in inducing the oligomerization of ZAR1-RKS1-PBL2^{UMP} (fig. S2). Consistent with our biochemical data, AvrAC promoted ZAR1 self-interaction in protoplasts detected by co-immunoprecipitation (co-IP) assays (fig. S3). Collectively, the results from our biochemical and cell-based assays indicate that AvrAC induces the formation of a dATP- or ATP-dependent oligomeric complex containing ZAR1, RKS1, and PBL2^{UMP}.

To reveal the structural basis of the AvrAC-induced oligomerization of ZAR1-RKS1-PBL2^{UMP}, we reconstructed the ZAR1 resistosome sample by cryo-EM (fig. S4, A and B). A total of 1,902,090 individual particles were used for reference-free two-dimensional (2D) classification (fig. S4C).

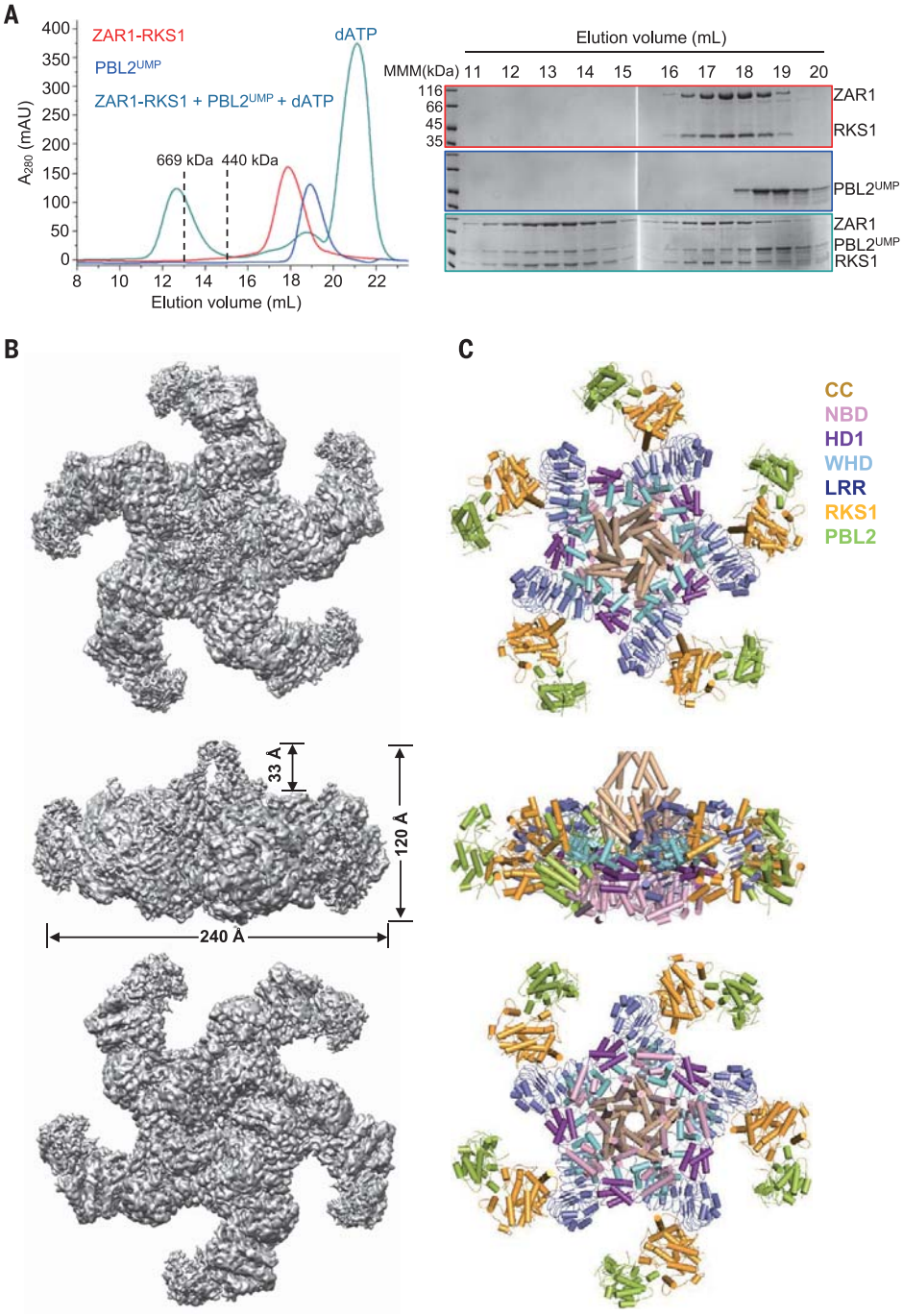

Fig. 1. In vitro reconstitution and 3D reconstruction of the ZAR1 resistosome. (**A**) PBL2^{UMP} binding induces oligomerization of the ZAR1-RKS1 complex in the presence of dATP (1 mM). (Left) Gel filtration profiles of ZAR1-RKS1, PBL2^{UMP}, and ZAR1-RKS1 with PBL2^{UMP} (ZAR1-RKS1+PBL2^{UMP}). Positions of standard molecular masses are indicated by dashed lines. A_{280}, absorbance at 280 nm; mAU, milli–absorbance units. (Right) Peak fractions in the left panel were visualized by SDS–polyacrylamide gel electrophoresis (PAGE) followed by Coomassie-blue staining. The ZAR1 resistosome refers to the oligomerized ZAR1-RKS1-PBL2^{UMP} complex. MMM, molecular mass markers. (**B**) The final 3D reconstruction of the ZAR1 resistosome shown in three orientations. (**C**) Model of the ZAR1 resistosome in three orientations.

After 3D classification, a subset of 196,707 particles was used for reconstruction, yielding a final overall resolution of 3.4 Å on the basis of the gold Fourier shell correlation standard (fig. S4D).

The 3D reconstruction reveals that the ZAR1 resistosome contains five protomers of the ZAR1-RKS1-PBL2^{UMP} complex, forming a wheel-like structure measuring ~240 Å in diameter and ~120 Å in height (Fig. 1B, movie S1, and table S1). This structure is reminiscent of those of the NLR inflammasomes (*18*–*20*) and apoptosomes (*17*). The ZAR1 resistosome is composed of a central α-helical barrel that is formed by the CC domains of ZAR1 (ZAR1^{CCs}). A small fraction of the barrel protrudes out of the wheel-defined plane and points toward the solvent region (Fig. 1C). The NB-ARC domains, which can be further divided into the NBD (ZAR1^{NBD}), HD1 (ZAR1^{HD1}), and WHD (ZAR1^{WHD}), form an outer ring structure (Fig. 1C). The bottom and the top of the ring are generated by lateral packing of ZAR1^{NBDs} and alternating contacts between ZAR1^{HD1} and ZAR1^{WHD} in adjacent subunits, respectively. The pentagonal chamber formed on the top is lined with most of the ZAR1^{CC}-made barrel (Fig. 1C). The LRRs do not pack against each other but make lateral contacts with ZAR1^{HD1}, thus contributing to the pentamerization of the ZAR1 resistosome. RKS1 and PBL2^{UMP} extend radially to form the spokes of the wheel-like structure, and neither of them is involved in the oligomerization of the resistosome (Fig. 1C). Structural comparison showed that the interaction of ZAR1^{LRR} with RKS1-PBL2^{UMP} remains unchanged during activation (figs. S5 and S6). For this reason, we limit our discussions below to ZAR1.

Release of the very N-terminal α helix during ZAR1 activation

The NBD, HD1, and WHD in the ZAR1 resistosome are organized similarly to those in active Apaf-1 and NLRC4 (fig. S7), indicating that ZAR1 adopts an active conformation. By contrast to the active NLRC4 and Apaf-1, which have an extended conformation, the active ZAR1 is largely spherical (fig. S7). Comparison with the structure of inactive ZAR1 (*34*) showed that ZAR1^{WHD} and ZAR1^{LRR} undergo little change relative to each other during activation (Fig. 2A and fig. S8). By contrast, structural remodeling occurs between these two structural domains and ZAR1^{NBD}-ZAR1^{HD1}, with the former two rotating ~180 degrees around the hinge (residues 393 to 395) linking ZAR1^{HD1} and ZAR1^{WHD} (Fig. 2A). Similar conformational changes were also observed for the activation of Apaf-1 (*17*) and NLRC4 (*18*–*20*). Structural superposition of the inactive ZAR1 with one protomer of a lateral ZAR1 dimer revealed that ZAR1^{CC}, ZAR1^{WHD}, and ZAR1^{LRR} from the inactive ZAR1 overlap with the other ZAR1 protomer (Fig. 2B), suggesting that the three domains have a role in sequestering ZAR1 in a monomeric state and explaining why structural reorganization is required for ZAR1 activation.

In addition to the structural reorganization of ZAR1^{NB-ARC}, conformational changes also take place in ZAR1^{CC} (residues 4 to 138) during activation. In the inactive ZAR1, the N-terminal amphipathic helix α1 is largely buried by the formation of a four-helix bundle and contacts with ZAR1^{WHD} and ZAR1^{LRR} (Fig. 2A, left). In the active ZAR1, this α helix detaches from the original four-helix bundle, rotating about 130 degrees around residue Asp^{25} and becoming fully solvent-exposed (Fig. 2A, right). The original α4A (residues 89 to 111) in the inactive ZAR1 becomes completely disordered in the active ZAR1, whereas the flexible fragment (residues 112 to 138) C terminal to the molten α helix folds into a long helix (α4B) during activation (Fig. 2C and fig. S9). Together with α2 and α3, this newly formed α helix forms a twisted three-helix bundle with its hydrophobic core partially buried. These structural observations indicate that ZAR1^{CC} (residues 1 to 138) can adopt two different fold topologies and that large structural rearrangement of other domains of ZAR1 during activation switches from one fold to the alternate one, a phenomenon called protein metamorphosis (*38*). The structure of ZAR1^{CC} in the resistosome is different from those of the CC domains of the CC-NLRs Sr33 (*39*), Rx (*40*), and MLA10 (*26*, *39*) (fig. S10).

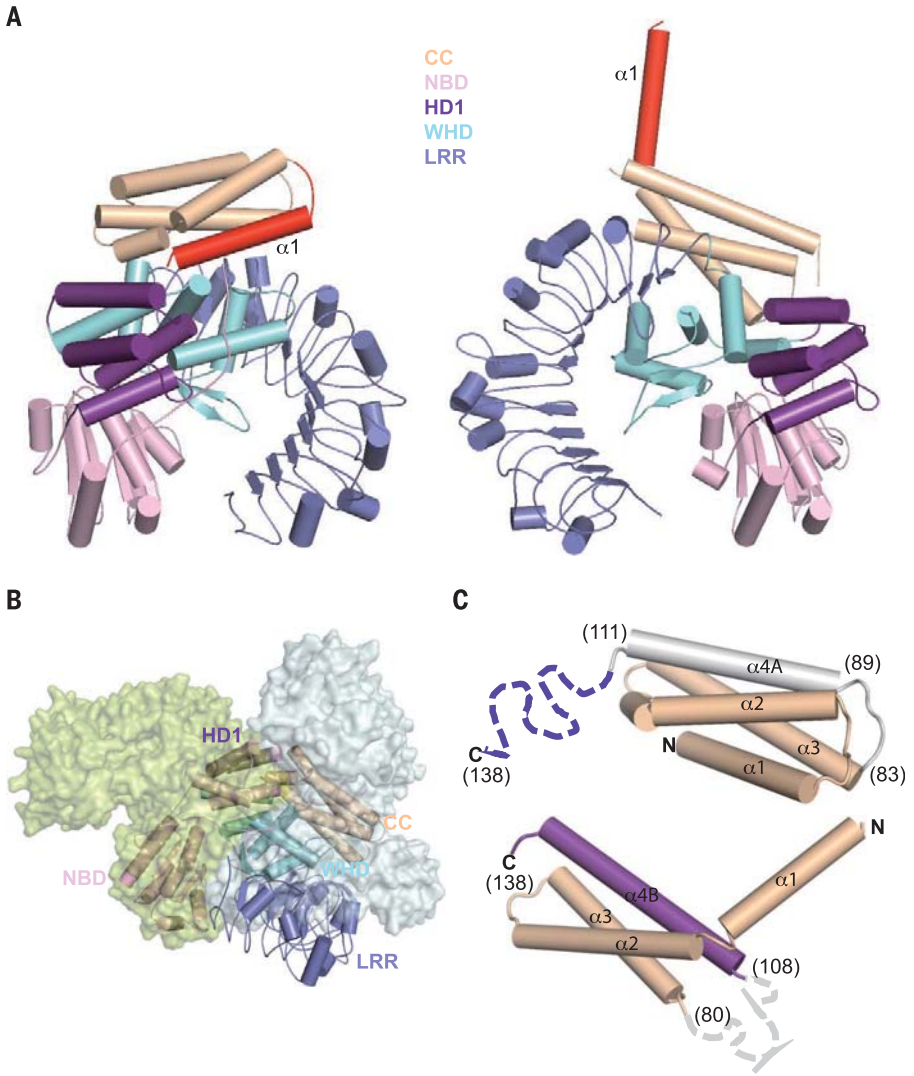

Fig. 2. Structural remodeling and fold switching of ZAR1 during activation. (**A**) Structural remodeling of ZAR1 during activation. Shown on the left and right are the inactive and active forms of ZAR1, respectively. The very N-terminal α helix (α1) is shown in red. The software Coot was used to align the two structures, with the inactive ZAR1^{NBD}-ZAR1^{HD1} as the template. (**B**) The CC, winged-helix, and LRR domains from the inactive ZAR1 overlap with one protomer of ZAR1 from a lateral dimer. ZAR1^{NBD}-ZAR1^{HD1} from the inactive ZAR1 (in cartoon representation) was used as the template to superimpose with the left protomer of the ZAR1 lateral dimer (in surface representation). (**C**) Structural comparison of the CC domain from the inactive (top) and active (bottom) forms of ZAR1. Secondary structural elements are labeled, and the boundaries for some of them are indicated by the numbers. Broken lines represent flexible structural elements.

Oligomerization of the resistosome mediated by ZAR1^{NBD}, ZAR1^{HD1}, ZAR1^{WHD}, and ZAR1^{LRR}

In the resistosome, all the subdomains of ZAR1 are involved in forming the stacking interactions between adjacent ZAR1 protomers (Fig. 1C). Additionally, a dATP molecule binds to the interface formed by ZAR1^{NBD} and ZAR1^{HD1} (Fig. 3A). The γ-phosphate group of the bound dATP forms an Arg^{297}-mediated hydrogen bond with Ser^{403} from ZAR1^{WHD}, thus stabilizing the active conformation of ZAR1 (Fig. 3B). Lateral ZAR1^{NBD}-ZAR1^{NBD} interaction is mediated mainly by packing of the N-terminal loop region (residues 148 to 156) from one ZAR1 protomer against two α helices from the other one (Fig. 3, A and C). Located at the center of this interface is Trp^{150} from the loop region, which forms hydrophobic and polar interactions with its neighboring residues from the other protomer (Fig. 3C). In addition to interacting with the loop region, one of the two helices also contacts an α helix from the other subunit via mainly polar interactions. The interface between the WHD of one ZAR1 protomer and HD1 of an adjacent protomer is also rich in polar interactions (Fig. 3D). Besides ZAR1^{NBD}, ZAR1^{HD1}, and ZAR1^{WHD}, ZAR1^{LRR} also participates in the pentamerization of the resistosome (Fig. 3, A and E). One lateral side of this domain establishes dense interprotomer interactions with one end of ZAR1^{HD1} through hydrophobic and van der Waals contacts. By contrast, only marginal interprotomer interactions occur between ZAR1^{NBD} and ZAR1^{WHD}.

To corroborate the structural observations, we generated four mutations, including three [ZAR1 S^{152}→E (ZAR1^{S152E}), ZAR1^{V154E}, and ZAR1^{W150A}] in the ZAR1^{NBD}-ZAR1^{NBD} interface (Fig. 3C) and one [the double mutation ZAR1 R^{149}→A and R^{297}→A (ZAR1$^{R149A/R297A}$)] in the dATP binding site (Fig. 3B) (single-letter amino acid abbreviations are defined in the legend to Fig. 3). We then individually purified these ZAR1 mutant proteins in complex with RKS1 from insect cells and examined their activity of oligomerization in the presence of PBL2^{UMP} and dATP by using gel filtration. In support of our structure, these four mutations substantially reduced the oligomerization of ZAR1 in the gel filtration assays (Fig. 3F). By contrast, the ZAR1^{T158E} mutation, which is located outside the oligomerization interface, had little effect on the oligomerization activity of ZAR1. We next investigated the cell death activity of these ZAR1 mutants in *Arabidopsis* protoplasts by using the assays we established previously (*32*). Consistent with the biochemical data, the ZAR1 mutants displaying abrogated or reduced oligomerization activity but not the ZAR1^{T158E} mutant were compromised in their ability to mediate cell death in protoplasts (Fig. 3G). We further complemented the *zar1* mutant plants by transforming them with the *ZAR1^{S152E}*, *ZAR1^{V154E}*, or *ZAR1$^{R149A/R297A}$* mutant under the control of the *ZAR1* native promoter and inoculated the resulting transgenic plants with wild-type *X. campestris* pv. *campestris* (*Xcc*8004) or an *X. campestris* pv. *campestris* (*Xcc*) strain lacking *avrAC* (Δ*avrAC*). Supporting the data from the biochemical and cell-based assays, wild-type Col-0 plants and *zar1* transgenic plants carrying wild-type *ZAR1* were fully resistant to *Xcc*8004 and displayed no disease symptoms, whereas *zar1* transgenic plants carrying the ZAR1^{S152E}, ZAR1^{V154E}, or ZAR1$^{R149A/R297A}$ variant developed typical disease symptoms indistinguishable from those of nontransgenic *zar1* plants (Fig. 3H and fig. S11). All plants developed disease symptoms in response to the Δ*avrAC* strain, indicating that the observed resistance is triggered only upon recognition of *avrAC*. Taken together, our data support an essential role of ZAR1 oligomerization in resistance to *Xcc* disease.

Oligomerization of ZAR1^{CC}

In the ZAR1 resistosome, the twisted three-helix bundles from the CC domains pack against each other. This results in the formation of an α-helical barrel (Fig. 4A) with its bottom interacting with the chamber formed by ZAR1^{WHD} and ZAR1^{LRR} (fig. S12). The helical barrel comprises two concentric rings, with α4B forming the inner ring and α2 and α3 forming the outer ring (Fig. 4A). The α-helical barrel of ZAR1^{CC} is reminiscent of that of the pentameric HIV-1 capsid protein (*41*) (fig. S13). Despite marginal interactions among the N-terminal five α helices of the ZAR1^{CCs}, these helices are configured into a funnel-shaped structure that protrudes out of the wheel-defined plane (Figs. 1C and 4A). The pore formed in the funnel-shaped structure has positive, negative, and neutral electrostatic potentials at its periphery, lumen, and outer surface, respectively (Fig. 4B). The inner diameter of the pore measures between ~30 Å at the bottom vestibule and ~10 Å at its narrowest constriction on the top. This axial pore is connected to the large interior space formed by the two tapered cylinder-shaped portions of the oligomeric CC domains. This space is likely solvent accessible, because a large window exists between two neighboring CC domains around their middle regions (Fig. 4A, bottom).

One oligomerization surface mediating the pentamerization of the CC domains results from the interaction of the exposed hydrophobic groove made by α2 and α4B with the C-terminal side of α4B from an adjacent subunit (called α4B′) (Fig. 4C, top). Centered at this interface are the aromatic residues Tyr^{132}, Phe^{135}, and Ile^{136} from α4B′, which make extensive hydrophobic contacts with their neighboring residues from α2 and α4B (Fig. 4C, top). Interactions from this oligomerization surface result in the formation of an intertwined four-helix bundle comprising α2, α3, α4B, and α4B′. The second oligomerization surface comes from packing of α3 and α4B against α2 from the other adjacent subunit (called α2′), forming an intertwined three-helix bundle (Fig. 4C, bottom). These structural analyses show that the surface of the three-helix bundle newly created during ZAR1 activation (Fig. 2C, bottom) is required for ZAR1^{CC} oligomerization. In support of the structural observations, ZAR1^{I136E}, predicted to perturb the first interface, substantially impaired the oligomerization of the mutant proteins in gel filtration (Fig. 4D). Consistently, the ZAR1^{I136E} mutant was compromised in mediating AvrAC-induced cell death in protoplasts (Fig. 4E). Transformation of *zar1* mutant plants with *ZAR1^{I136E}* failed to restore resistance to *Xcc*8004 (Fig. 4F and fig. S14), indicating that Ile^{136} is essential for immune signaling. These data agree with the finding that multiple sites within the CC domains of RPM1 and Sr33 contribute to self-association and HR (*39*, *42*).

Structural differences between the ZAR1 resistosome and inflammasomes or apoptosomes

Despite their different oligomerization states, the ZAR1 resistosome, the Apaf-1 and CED-4 apoptosomes, and the NLRC4 inflammasome form a wheel-like structure (Fig. 5). The NBD, HD1, and WHD are similarly positioned to mediate the oligomerization of ZAR1, Apaf-1, and NLRC4 (fig. S7). Like cytochrome *c* and WD40 domains in the Apaf-1 apoptosome, RKS1 and PBL2^{UMP} are not directly involved in the formation of the ZAR1 resistosome (fig. S15). dATP in the Apaf-1 apoptosome (*17*) and the ZAR1 resistosome and ATP in the CED-4 apoptosome (*36*) play similar roles in stabilizing the active conformations. By contrast to the 1:9 or 1:10 stoichiometry between the ligand and NLRC4 in the NAIP-NLRC4 inflammasomes (*18*–*20*), PBL2^{UMP} and ZAR1-RKS1 in the resistosome form a stoichiometry of 1:1 in complex, similar to cytochrome *c* with Apaf-1 in the Apaf-1 apoptosome (*17*). These results suggest that ZAR1 activation resembles that of Apaf-1 but differs from the induced self-activation of NLRC4.

Despite the similarities shared by the ZAR1 resistosome, the NLRC4 inflammasome, and the Apaf-1 and CED-4 apoptosomes, substantial structural differences exist among them. Because of a more compact conformation of the active ZAR1, ZAR1^{LRR} contributes to the oligomerization of the resistosome by contacting ZAR1^{HD1} from an adjacent ZAR1 subunit (Figs. 3E and 5A). This interaction results in the wrapping of ZAR1^{LRR} around the oligomerized ZAR1$^{NB\text{-}ARCs}$ in the resistosome, making ZAR1^{WHD} much less solvent accessible than the WHDs in the apoptosomes (Fig. 5, B and C) or the inflammasome (Fig. 5D). The structural differences between the ZAR1 resistosome and the inflammasome or the apoptosomes also extend to their N-terminal domains. In both the caspase-9–free Apaf-1 apoptosome (*17*) and the caspase-1–free NLRC4 inflammasome (*18*–*20*) in the absence of interacting partners, the N-terminal CARDs are completely disordered. The flexible oligomerized CARDs in the Apaf-1 apoptosome and the NLRC4 inflammasome appear to be compatible with their role in recruiting downstream caspase-9 and caspase-1, respectively. By contrast, the oligomeric CC domains in the ZAR1 resistosome are well defined and form an α-helical barrel (Fig. 5A). Unlike the fully exposed CARDs in the caspase-9–bound Apaf-1 apoptosome and the CED-4 apoptosome, which are located on the tops

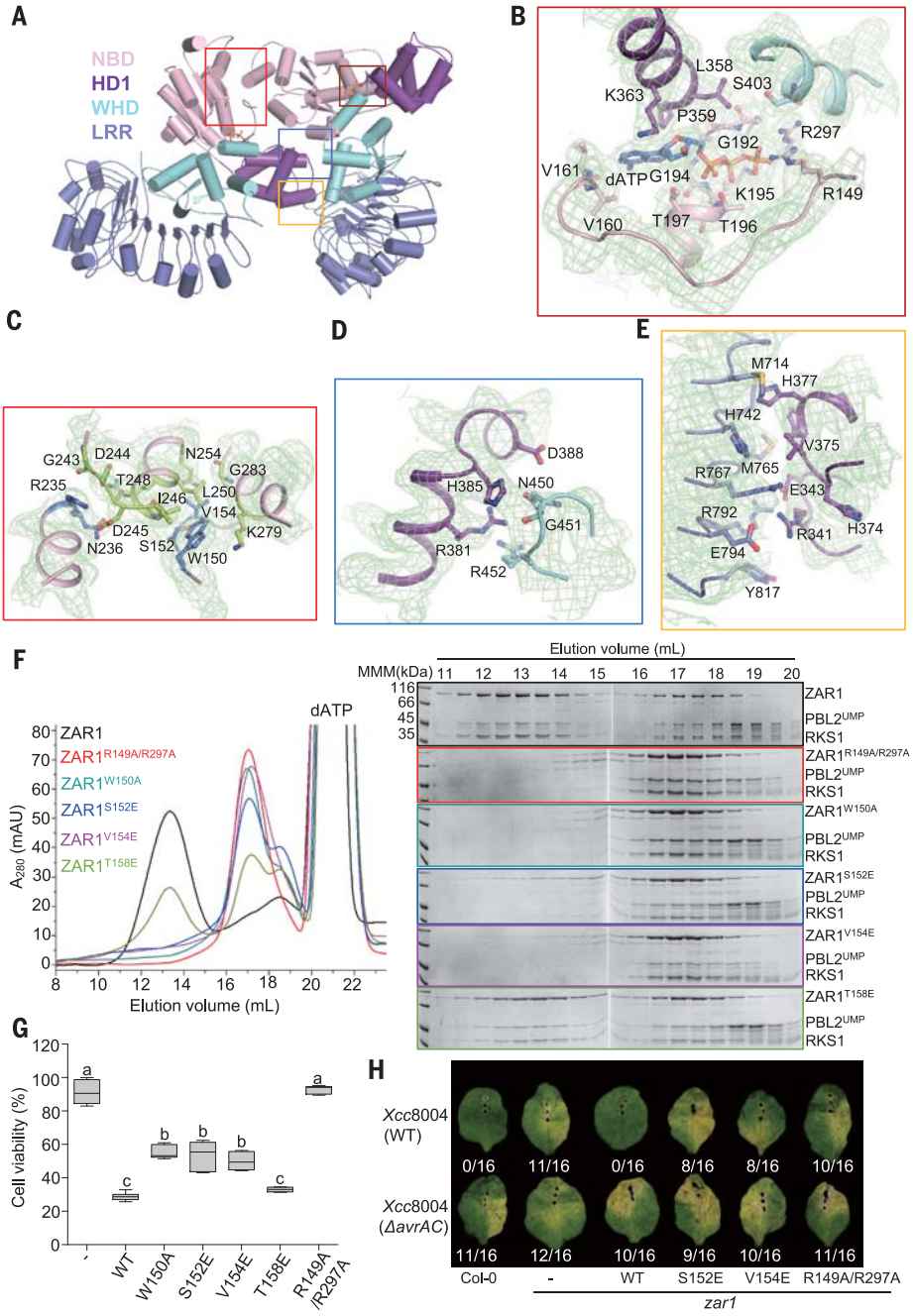

Fig. 3. Oligomerization of the ZAR1 resistosome is critical for ZAR1 functions. (**A**) A lateral ZAR1 dimer from the resistosome. The open frames highlight the interfaces mediating the lateral dimer. (**B**) Interaction between dATP and ZAR1. Cryo-EM density around the dATP binding site is shown as green mesh. Single-letter abbreviations for the amino acid residues are as follows: A, Ala; C, Cys; D, Asp; E, Glu; F, Phe; G, Gly; H, His; I, Ile; K, Lys; L, Leu; M, Met; N, Asn; P, Pro; Q, Gln; R, Arg; S, Ser; T, Thr; V, Val; W, Trp; and Y, Tyr. (**C** to **E**) Close-up views of the interaction highlighted in (A). (**F**) Mutations compromise the formation of the ZAR1 resistosome. (Left) Gel filtration profiles of ZAR1-RKS1 with PBL2^{UMP} are color coded to show different ZAR1 mutant proteins. (Right) Peak fractions in the left panel were visualized by SDS-PAGE followed by Coomassie-blue staining. (**G**) Compromising the formation of the ZAR1 resistosome impairs AvrAC-induced cell death in protoplasts. *zar1* protoplasts were cotransfected with AvrAC, PBL2, RKS1, and various ZAR1 constructs as indicated. A protoplast viability assay was performed for the transfected protoplasts. Data are represented as the mean ± SE (n = 6). Different letters indicate significant difference ($P \leq 0.05$; Tukey test). The experiments were performed three times with similar results. WT, wild type. (**H**) Formation of the ZAR1 resistosome is required for AvrAC-induced resistance to *Xcc*. *zar1* plants complemented with the constructs indicated were infiltrated with wild-type *Xcc*8004 or *Xcc*8004 Δ*avrAC*. Disease symptoms were scored 7 days after inoculation. Numbers indicate the ratio of leaves developing chlorosis to the total number of inoculated leaves. The experiments were repeated twice with similar results.

of the central hubs (Fig. 5, B and C), the α-helical barrel in the ZAR1 resistosome is positioned at the bottom of the wheel-like structure (Fig. 5A), and the bulk of it interacts with the chamber formed by the oligomerized ZAR1^{LRR} and ZAR1^{WHD}. This interaction results in the complete burial of one end of the oligomerized NBDs from the ZAR1 resistosome (Fig. 5A).

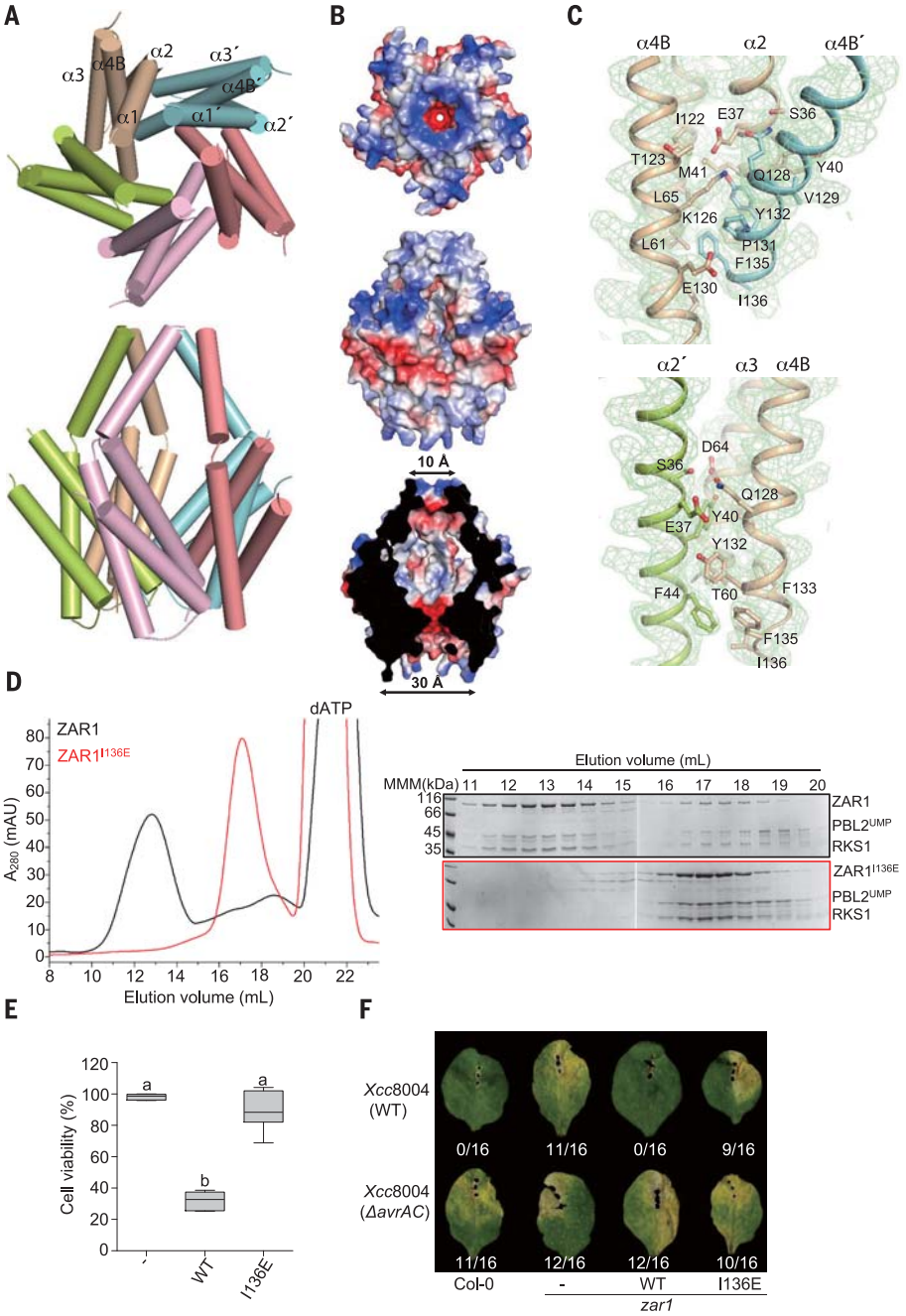

Fig. 4. The ZAR1^{CC}-constructed helical barrel is critical for ZAR1 functions. (**A**) Top (top) and side (bottom) views of the helical barrel formed by ZAR1^{CC} in the ZAR1 resistosome. (**B**) Electrostatic surface potentials of the helical barrel. Shown are top (top) and side (middle) views of the potentials. The bottom shows a cut-through of the side view. (**C**) Detailed ZAR1^{CC}-ZAR1^{CC} interactions in the helical barrel. (**D**) ZAR1^{I136E} impairs PBL2^{UMP}-induced oligomerization of ZAR1-RKS1. The assays were performed as described for Fig. 3F. (**E**) ZAR1^{I136E} has lower activity in mediating AvrAC-induced cell death in protoplasts. The assays were performed as described for Fig. 3G. Data are represented as the mean ± SE. Different letters indicate significant difference ($P \leq 0.05$; Tukey test). (**F**) ZAR1^{I136E} has lower activity in mediating AvrAC-induced disease resistance. The assays were performed as described for Fig. 3H. Numbers indicate the ratio of leaves developing chlorosis to the total number of inoculated leaves.

The amphipathic helix required for plasma membrane association and immunity

Ectopic expression of ZAR1^{CC} is sufficient to recapitulate the cell death activity of full-length ZAR1 (*43*). Most of the oligomerized CC domain in the ZAR1 resistosome, however, is substantially buried, except for the funnel-shaped structure formed by the oligomerized N-terminal amphipathic α1 (Fig. 1C). These observations suggest that the very N-terminal amphipathic helix can be essential for the cell death activity of ZAR1. To test this hypothesis, we first investigated the effect of N-terminal deletions on ZAR1-mediated cell death in protoplasts. In full support of our hypothesis, N-terminal deletion of the first 6 (ZAR1^{Δ6}), 10 (ZAR1^{Δ10}), or 23 (ZAR1^{Δ23}) residues abolished the cell death activity of ZAR1 in protoplasts (Fig. 6A, top). A similar effect was also observed for the triple mutation ZAR1$^{F9A/L10A/L14A}$, which is located at the outer surface of the funnel-shaped structure (Fig. 6A, bottom), providing further evidence for an indispensable role of the N-terminal amphipathic helix in ZAR1-mediated cell death. In addition, N-terminal fusion of the FLAG tag also inactivated ZAR1 cell death activity (Fig. 6B), suggesting that a free N terminus of ZAR1 is required for its cell death activity. We further tested the ability of ZAR1^{Δ10} and ZAR1$^{F9A/L10A/L14A}$ to confer resistance to *Xcc*8004 by transforming *zar1* mutant plants. Consistent with the protoplast data, neither mutant transgene conferred resistance to *Xcc*8004 (Fig. 6C and fig. S16). However, α1 of ZAR1^{CC} makes only a marginal contribution to the oligomerization of the ZAR1 resistosome (Fig. 1C). Co-IP assays detected ZAR1^{Δ10}-ZAR1^{Δ10} interaction that was enhanced by AvrAC compared with that obtained with the AvrAC^{H469A} mutant (Fig. 6D). Similarly, the ZAR1$^{F9A/L10A/L14A}$ mutant still retained normal interaction with RKS1, AvrAC-induced interaction with PBL2, self-association, and oligomerization in gel filtration (fig. S17). By contrast, the AvrAC-induced self-association of ZAR1 was abolished by ZAR1^{K195N} at the P loop and ZAR1$^{R149A/R297A}$ in co-IP assays (Fig. 6D), a result consistent with the notion that AvrAC-induced ZAR1 oligomerization in the plant cell requires Lys^{195}, Arg^{149}, and Arg^{297}. Collectively, these results show that the functionally essential N-terminal helix is dispensable for the assembly of an oligomeric ZAR1 complex, suggesting that the funnel-shaped structure has other biochemical activity required for ZAR1-mediated cell death.

Several CC-NLRs, including RPM1 (*42*, *44*), RPS2 (*45*), RPS5 (*46*), and Tm-2^2 (*47*), have been shown to associate with the plasma membrane (PM), and the PM localization is required for their HR activity. We therefore investigated whether ZAR1 is PM associated by using the assays described previously (*47*). A small amount of ZAR1 was detected in the PM when ZAR1 was coexpressed with the AvrAC^{H469A} mutant, suggesting that inactive ZAR1 has a weak PM association activity. This result is consistent with what has been observed with inactive RPM1 (*44*) and Tm-2^2 (*47*). By comparison, the PM association

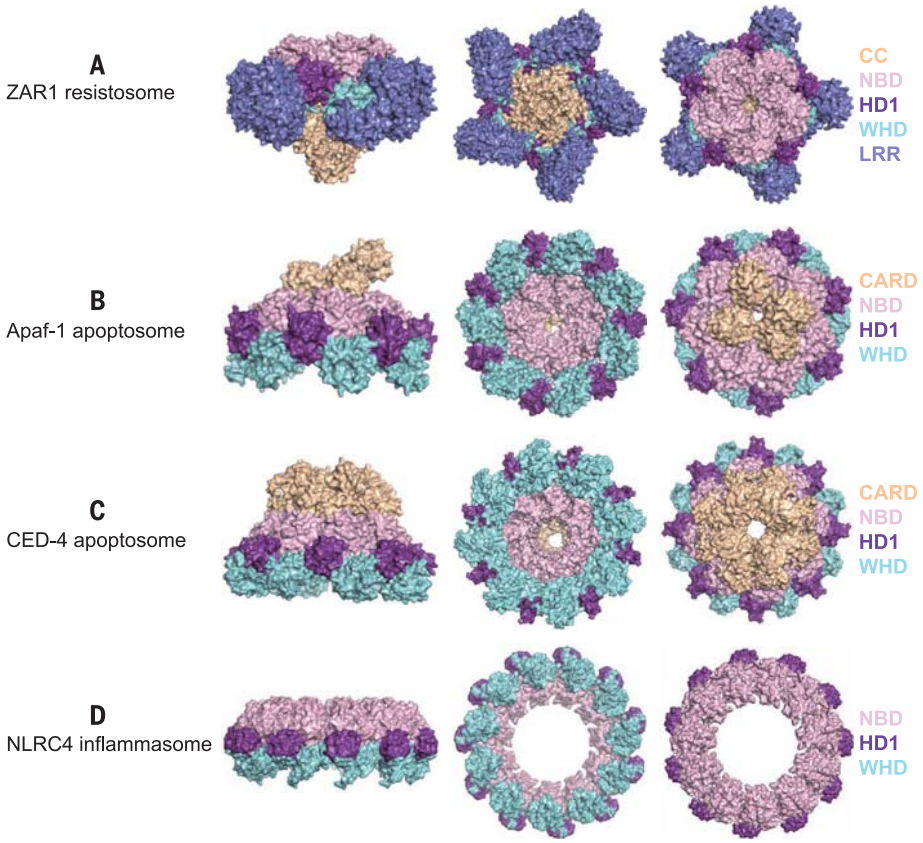

Fig. 5. Comparison of the ZAR1 resistosome with apoptosomes or an NLR inflammasome. (**A** to **D**) The structures (in surface representation) of the ZAR1 resistosome, the Apaf-1 apoptosome, the CED-4 apoptosome, and the NLRC4 inflammasome. The structures are not on the same scale. The first, second, and third columns show the side, bottom, and top views of these structures, respectively.

activity of ZAR1 was enhanced when ZAR1 was coexpressed with wild-type AvrAC, as indicated by a much larger amount of ZAR1 in the PM (Fig. 6E). These results indicate that AvrAC uridylyltransferase activity facilitates ZAR1 association with the PM, likely through inducing the oligomerization of the NLR protein. The AvrAC-induced ZAR1-PM association was compromised in the ZAR1^{K195N} and ZAR1$^{R149A/R297A}$ mutants (Fig. 6E), both of which lost cell death activity in protoplasts (*32*) (Fig. 3G). Furthermore, the N-terminally FLAG-tagged ZAR1 also had a lower level of AvrAC-induced PM association, indicating that the perturbation of α1 in ZAR1^{CC} impairs PM association (Fig. 6E). These results collectively support the idea that AvrAC-induced ZAR1^{CC} α1 rearrangement and PM association are required for the immunity conferred by ZAR1.

The inner surface of the funnel-shaped structure contains several negatively charged residues (Fig. 6A, bottom). Simultaneous mutation of two such residues, Glu^{11} and Glu^{18}, greatly reduced the ZAR1-mediated cell death activity in protoplasts (Fig. 6A, top) and resistance to *Xcc*8004 disease in transgenic plants (Fig. 6C, bottom). The ZAR1$^{E11A/E18A}$ mutation did not affect the AvrAC-induced PM association (Fig. 6E), indicating that the AvrAC-induced PM association is required but not sufficient for the immune function of ZAR1.

Discussion

Despite intense studies of plant NLRs during the past two decades, the biochemical mechanisms of their activation are still poorly understood, and little is known about their immediate postactivation signaling. Our structural, biochemical, and functional data provide information regarding the molecular mechanisms for the activation and assembly of an active structure in a plant NLR protein. The successful in vitro reconstitution of the ZAR1 resistosome opens opportunities for further biochemical characterization of activated plant NLR proteins. The structural differences between the ZAR1 resistosome and the NLRC4 inflammasome or the Apaf-1 apoptosome around the N-terminal CARDs suggest different NLR signaling mechanisms between plants and animals.

PM association required for ZAR1-mediated cell death and disease resistance

Structural remodeling and fold switching during activation results in the detachment of the very N-terminal amphipathic helix from the core of ZAR1^{CC} (Fig. 2A). Functional studies support an indispensable role of this helix in AvrAC-induced PM association, cell death, and disease resistance (Fig. 6). These results collectively indicate that AvrAC-induced activation converts ZAR1 from a cytosolic state into a PM-associated state to mediate cell death and disease resistance. The PM localization of RPM1, TM-2^2, and RPS5 is P-loop dependent, and their autoactive mutants are primarily PM localized (*42*, *46*, *47*). In sharp contrast, the inactive K191R P-loop mutant of TM-2^2 is largely soluble (*47*), similar to the ZAR1^{K195N} mutant (Fig. 6E). Unlike ZAR1, however, both resting and active RPM1 and TM-2^2 were shown to be PM localized, suggesting that PM localization is insufficient for their activation. It may be that ligand-induced conformational changes in or oligomerization of these two NLR proteins in the PM is required for their activation. Whether they form structures similar to that of the ZAR1 resistosome remains to be determined. In addition to interaction with α2 and α3, the N-terminal amphipathic helix is further sequestered through interaction with ZAR1^{WHD} and ZAR1^{LRR} in the inactive ZAR1^{CC} domain (Fig. 2A). Thus, structural remodeling and fold switching function to release the latent PM association and immune signaling activities encoded within ZAR1^{CC}. Oligomerization of the released N-terminal amphipathic helices results in the formation of a funnel-shaped structure in the ZAR1 resistosome (Fig. 4A) that is required for the PM association and immune function of ZAR1 (Fig. 6). Mechanistically, the assembly of the funnel-shaped structure from the ZAR1 resistosome resembles that of the hemolytic pore-forming protein fragaceatoxin C (FraC) (*48*) (fig. S18), although the two proteins share little structural similarity. Formation of the fully assembled pore of FraC also involves conversion from a soluble to a PM-associated form. Conformational changes in the funnel-like structure are possible after binding of the ZAR1 resistosome to the PM.

Biochemical functions of the ZAR1 resistosome

Currently, the precise biochemical functions of the ZAR1 resistosome remain unclear. It is possible that the oligomeric CC domains of the ZAR1 resistosome recruit unknown components to trigger HR cell death signaling. However, the well-defined but largely buried CC pentameric structure in the ZAR1 resistosome contrasts with the flexible CARDs in the Apaf-1 apoptosome and the NLRC4 inflammasome (Fig. 5) and belies a scaffolding role of this structural portion of the ZAR1 resistosome. A nonscaffolding role of the funnel-shaped structure in ZAR1-mediated cell death is consistent with the observation that a ZAR1$^{E11A/E18A}$ double mutation of its inner surface, which is unlikely to affect potential interactions with other proteins, impaired the cell death activity and disease resistance function of ZAR1 (Fig. 6, A and C). This result also suggests that the interior space of the funnel structure is required for ZAR1-mediated cell death, though the underlying mechanism remains unclear. A more attractive alternative, but not necessarily

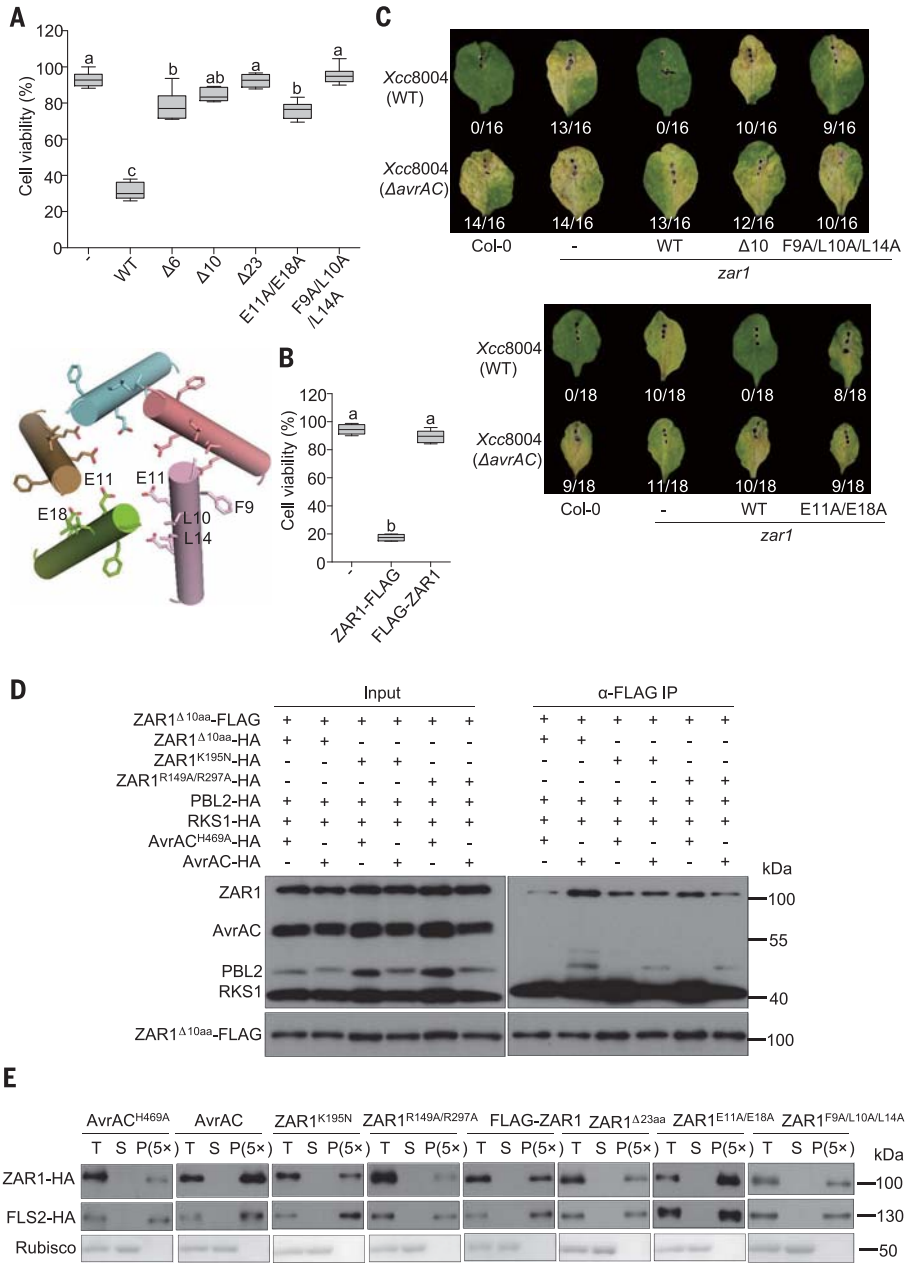

Fig. 6. α1 is required for AvrAC-induced cell death and PM association of ZAR1. (**A**) (Top) Mutations of the very N-terminal α helix of ZAR1 reduce AvrAC-induced cell death in protoplasts. The assays were performed as described for Fig. 3G. (Bottom) Structure of the N-terminal α helices in the ZAR1 resistosome. (**B**) A FLAG tag fused to the N terminus of ZAR1 inactivates the cell death activity of ZAR1 in protoplasts. Data in (A) and (B) are represented as the mean ± SE. Different letters indicate significant difference ($P \leq 0.05$; Tukey test). (**C**) ZAR1 mutants with the first 10 residues deleted, with three residues mutated, or with the mutations E11A and E18A are compromised in their ability to restore the resistance of *zar1 Arabidopsis* to *Xcc*. The assays were performed as described for Fig. 3H. Numbers indicate the ratio of leaves developing chlorosis to the total number of inoculated leaves. (**D**) The ZAR1$^{\Delta 10}$ mutant retains AvrAC-induced self-association activity. Protoplasts were transfected with the indicated constructs, and total protein was isolated for co-IP assays. The experiments were performed three times with similar results. aa, amino acids. (**E**) The very N-terminal α helix is critical for the AvrAC-enhanced PM association. Protoplasts with a *zar1* background were transfected with the indicated constructs. Total protein (T) was extracted and separated into soluble (S) and PM (P) fractions by using the Minute PM protein isolation kit, and protein was detected by anti-HA or anti-FLAG immunoblotting. P(5×) indicates five times enrichment relative to T or S. The experiments were performed three times with similar results.

exclusive with the above hypothesis, is that the funnel-shaped structure of the ZAR1 resistosome can be per se membrane spanning, thus directly influencing PM permeability or perturbing its integrity or both to initiate cell death and immune signaling. Evidence for RPS2 as an integral protein has been provided in vivo (*49*, *50*), although whether its activation affects the PM localization remains unknown. This model predicts that a free N terminus of ZAR1 is essential for its functions. N-terminal fusion and deletion abolished the AvrAC-induced PM association and cell death activities of ZAR1 (Fig. 6). Similar results were also obtained with the CC-NLRs MLA1 and MLA6 (*51*). Furthermore, N-terminal fusion with green fluorescent protein completely inactivated the cell death activity of the autoactive D485V mutant of the CC-NLR Pit from rice (*52*). Cell death through CC domain–perturbed PM integrity is in line with the observations that ion fluxes across the PMs of lettuce cells are one of the earliest cellular events during effector-triggered immunity against the oomycete *Bremia lactucae* pathogen and that irreversible membrane damage is a key signaling event leading to HR cell death (*53*). This would also imply the existence of a highly conserved signaling mechanism downstream of CC-NLR across different phylogenetic lineages of plants. HR-like cell death in plants can also be induced by the expression of some pore-forming proteins, such as the harpin protein HrpZ1 (*54*) from the plant pathogen *Pseudomonas syringae*, a bacterial proton pump (*55*), and the proapoptotic protein BAX from animals (*56*). Inducible pores and ion channels in animals were recently shown to be the executors of pyroptosis (*57*–*59*) and necroptosis (*60*–*62*), respectively. Thus, it appears that alterations of PM integrity or ion homeostasis in the cytosol are a shared mechanism used by both animals and plants for the execution of cell death. Whether the AvrAC-induced structural changes at the N terminus of ZAR1 activate defense by creating a new docking site for signaling proteins or whether the restructured N terminus exerts direct effects on plant membranes remains to be determined.

Implications in the activation of other plant NLRs

The present study supports the AvrAC-induced oligomerization of ZAR1-RKS1-PBL2^{UMP} into the ZAR1 resistosome in the presence of dATP or ATP, further confirming oligomerization as a hallmark of AAA+ ATPases (*9*, *63*). Although whether other plant NLRs similarly form resistosomes upon activation remains unknown, studies of plant NLRs have suggested that they oligomerize during activation as well (*64*, *65*). Although the NB-ARC domain of ZAR1 is more similar to those of plant NLRs than to those of NLRC4 and Apaf-1 (fig. S19) in amino acid sequence, the NBDs, HD1s, and WHDs of ZAR1, NLRC4, and Apaf-1 are similarly positioned in their inactive (*34*) and active (Fig. 5) states. It therefore stands to reason that other plant NLRs would undergo structural remodeling like that

demonstrated in ZAR1 activation. In addition to the structural remodeling of the WHD relative to the NBD, ZAR1^{CC} undergoes fold switch during activation. The fold plasticity of the CC domain of an NLR protein does not appear to be limited to ZAR1. For instance, the CC domains of the wheat NLR Sr33 (residues 6 to 120) and barley NLR MLA10 (residues 5 to 120) display different fold topologies in nuclear magnetic resonance (*39*) and crystallography (*26*, *39*), which likely reflect fold switching of the CC domain by varying the conditions used for structural determination of these two nearly identical CC domains. Future studies will be needed to test whether the CC domains of MLA10 and other plant NLRs are metamorphic.

Like ZAR1, several other CC-NLRs, including RPM1, RPS2, TM-2^2, and RPS5, are PM localized. Furthermore, the CC domains of these CC-NLRs are required for their functions (*42*–*47*). These results suggest that these plant NLRs function in similar ways to trigger HR cell death and resistance. However, the CC domain of the potato CC-NLR Rx appears to be dispensable for signaling, because overexpression of the NBD but not the CC domain in *N. benthamiana* leaves induces an HR (*66*). Then how does this CC-NLR protein initiate immune signaling? Clues to the answer are provided by a recent study (*67*) showing that a subfamily of CC-NLRs called NRC (NLR required for cell death) is required for Rx-mediated resistance. Data from the same study suggested that Rx and other NRC-dependent NLR proteins positively regulate the immune activity of NRC. Furthermore, the P loop was shown to be essential for NRC4-mediated immunity. These results raise the possibility that NRCs function like ZAR1 to initiate immune signaling, a possibility to be rigorously tested in future studies.

Our findings may additionally shed light on immune signaling mediated by TIR-NLRs, as increasing evidence indicates that several classes of CC-NLRs function downstream of TIR-NLRs in immune signaling (*68*–*70*). One or both of the CC-NLRs NRG1 (N requirement gene 1) (*71*) and ADR1 (activated disease resistance 1) (*72*), belonging to the RPW8 clade (*25*), are required for the functions of TIR-NLRs in *Arabidopsis* and *N. benthamiana*. NRG1 is required for HR cell death but not resistance mediated by the RRS1-RPS4 pair (*71*). Overexpression of an N-terminal fragment (residues 1 to 182) terminating before the NBD of NRG1 constitutively induces HR in *N. tabacum*. As in ZAR1, N-terminal deletion of 13 residues completely abolishes the HR-inducing activity of the NRG1 fragment. The corresponding residues in RPW8 are believed to constitute a transmembrane domain (*73*). Furthermore, biochemical data suggested that P loop–dependent oligomerization of NRG1 is essential for HR triggering in *N. benthamiana* (*69*). These results raise the possibility that NRG1 acts like ZAR1 to execute cell death mediated by TIR-NLRs.

In summary, our data collectively support a model of AvrAC-induced activation of the ZAR1 resistosome (Fig. 7). The CC-dependent association of the ZAR1 resistosome with the PM may perturb PM integrity and/or ion homeostasis, which not only causes terminal cell death but additionally mediates rapid stress-induced transcriptional activation of defense genes. This is a scenario paralleling the immune response and pyroptosis mediated by the NLRC4 inflammasome and is consistent with the suggestion that components of HR cell death function to signal defense activation (*74*, *75*). Thus, the ZAR1 resistosome likely functions as an executor of cell death and indirectly regulates other downstream immune responses.

Materials and methods

ZAR1 and RKS1 (with an N-terminal six-His–SUMO tag) were coexpressed in Sf21 insect cells. The complex protein was first purified by using Ni–nitrilotriacetic acid and further cleaned by ion exchange and gel filtration chromatography after the removal of SUMO by PreScission. AvrAC and PBL2 (with a C-terminal six-His tag) were coexpressed in *Escherichia coli*, and the PBL2^{UMP} protein was purified by using the protocols described above. The purified ZAR1-RKS1 complex protein was then incubated with an excess amount

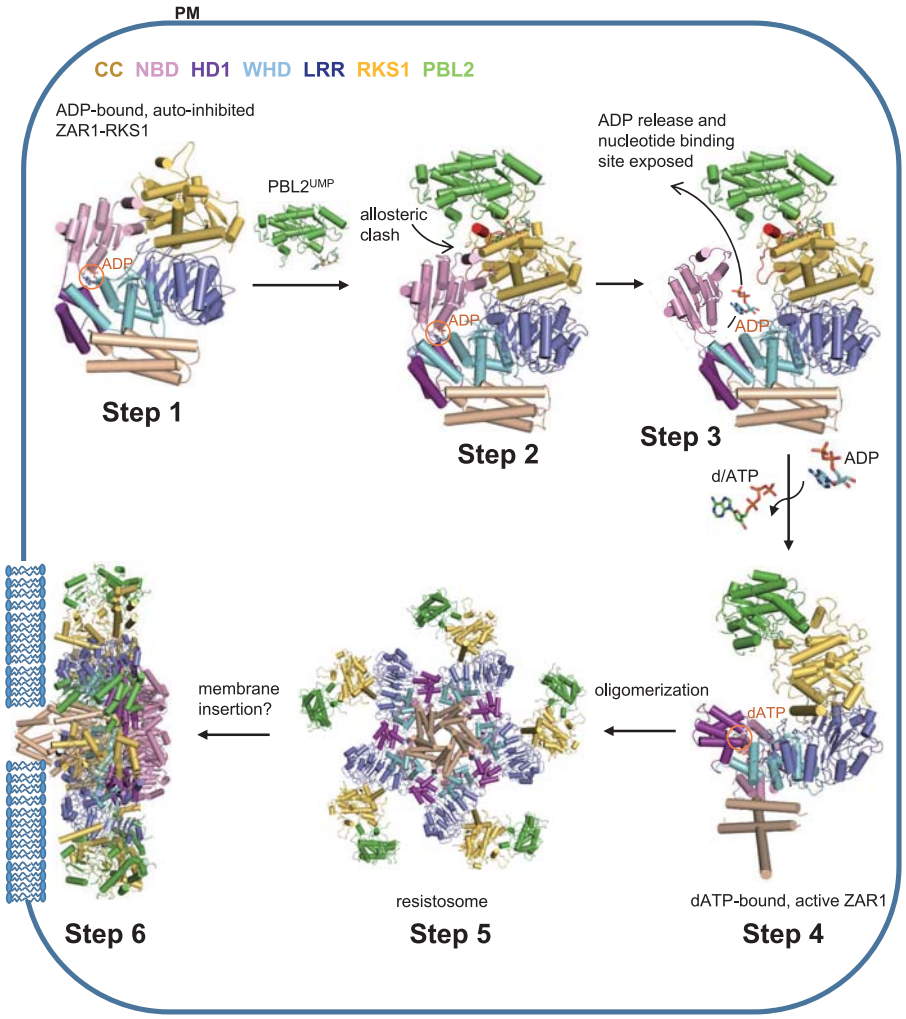

Fig. 7. Model of AvrAC-induced assembly of the ZAR1 resistosome. In the resting state, the preformed ZAR1-RKS1 complex is mediated by interaction between the LRR domain of ADP-bound ZAR1 and RKS1 (step 1). ZAR1 in the complex is maintained in an auto-inhibited state through intramolecular interactions of multiple domains. After pathogen infection, AvrAC uridylates PBL2, and the modified PBL2 (PBL2^{UMP}) then serves as a ligand to interact exclusively with RKS1 from ZAR1-RKS1 (step 2). PBL2^{UMP} binding activates the nucleotide exchange factor activity of RKS1 by stabilizing the activation segment of RKS1 (steps 2 and 3). Once activated, RKS1 facilitates ADP release from ZAR1 by inducing conformational changes in ZAR1^{NBD} (step 3), which enable ZAR1 to be primed and bind dATP or ATP. dATP or ATP binding further induces structural remodeling of ZAR1 and fold switching of its CC domain (step 4), resulting in the formation of a pentameric ZAR1-RKS1-PBL2^{UMP} complex (step 5), dubbed the ZAR1 resistosome. The funnel-shaped structure formed by the very N-terminal helices of ZAR1 in the resistosome promotes ZAR1 association with or integration into the PM (step 6). The PM-associated or integrated ZAR1 resistosome can function as a direct executor of cell death and/or an inducer of immune response by perturbing the PM integrity or ionic homeostasis.

of $PBL2^{UMP}$ at a molar ratio of ~1:2 and 1 mM dATP, ATP, or ADP at 4°C. To purify the ZAR1 resistosome protein, the mixture was concentrated and then subjected to gel filtration. Fractions corresponding to the ZAR1 resistosome were collected and concentrated to ~3.0 mg/ml for cryo-EM investigation. Similar protocols were used to purify ZAR1 mutants involved in oligomerization. To test the effect of mutations in ZAR1 on the assembly of the ZAR1 resistosome, a purified ZAR1-RKS1 mutant complex was incubated with an excess amount of $PBL2^{UMP}$, and the mixture was subjected to gel filtration.

Cryo-EM data from frozen hydrated grids of the ZAR1 resistosome were collected on a Titan Krios electron microscope operated at 300 kV and equipped with a Cs corrector and a Gatan Bioquantum energy filter with a K2 Summit direct electron detection camera (Gatan) by using AutoEMation. The raw supersolution dose-fractionated image stacks were binned, aligned, dose weighted, and summed by using MotionCor2. Contrast transfer function (CTF) parameters were estimated by using CTFFIND4. Particle picking, 2D classification, 3D classification, and refinement were all performed in RELION. $ZAR1^{LRR}$-$ZAR1^{WHD}$ and $ZAR1^{NBD}$-$ZAR1^{HD1}$ from the model of the ZAR1-RKS1 complex and RKS1-$PBL2^{UMP}$ from the model of the nucleotide-free ZAR1-RKS1-$PBL2^{UMP}$ complex were docked into the EM density of the ZAR1 resistosome in Chimera. Five dATP molecules were docked into the density in Coot. The model containing five dATP-bound ZAR1-RKS1-$PBL2^{UMP}$ molecules was refined against the EM map by PHENIX.

Structure-guided mutagenesis was carried out to assess the importance of various amino acid residues in ZAR1-ZAR1 interaction, cell death triggering, association with the PM, and resistance in plants. Wild-type and mutant ZAR1, RKS1, PBL2, and AvrAC constructs were transfected into *Arabidopsis* protoplasts, and cell viability was determined. ZAR1 variants under the control of the native promoter were introduced into *zar1* mutants, and stable transgenic plants were wound inoculated with *Xcc* strains carrying or lacking *avrAC*. Disease resistance was scored on the basis of the presence or absence of disease symptoms. ZAR1 variants containing a hemagglutinin (HA) or FLAG tag were coexpressed in *Arabidopsis* protoplasts, and co-IP was carried out to test the effects of ZAR1 mutations on ZAR1-ZAR1 interaction in plant cells. *Arabidopsis* protoplasts expressing the desired constructs were treated with $LaCl_3$ to inhibit cell death, and the PM was isolated. Amounts of ZAR1 protein associated with the PM were determined by immunoblot analysis.

REFERENCES AND NOTES

1. J. D. Jones, J. L. Dangl, The plant immune system. *Nature* **444**, 323–329 (2006). doi: 10.1038/nature05286; pmid: 17108957
2. T. Maekawa, T. A. Kufer, P. Schulze-Lefert, NLR functions in plant and animal immune systems: So far and yet so close. *Nat. Immunol.* **12**, 817–826 (2011). doi: 10.1038/ni.2083; pmid: 21852785
3. Q. Yin, T. M. Fu, J. Li, H. Wu, Structural biology of innate immunity. *Annu. Rev. Immunol.* **33**, 393–416 (2015). doi: 10.1146/annurev-immunol-032414-112258; pmid: 25622194
4. E. Meunier, P. Broz, Evolutionary convergence and divergence in NLR function and structure. *Trends Immunol.* **38**, 744–757 (2017). doi: 10.1016/j.it.2017.04.005; pmid: 28579324
5. Z. Duxbury *et al.*, Pathogen perception by NLRs in plants and animals: Parallel worlds. *Bioessays* **38**, 769–781 (2016). doi: 10.1002/bies.201600046; pmid: 27339076
6. P. N. Dodds, J. P. Rathjen, Plant immunity: Towards an integrated view of plant-pathogen interactions. *Nat. Rev. Genet.* **11**, 539–548 (2010). doi: 10.1038/nrg2812; pmid: 20585331
7. S. T. Chisholm, G. Coaker, B. Day, B. J. Staskawicz, Host-microbe interactions: Shaping the evolution of the plant immune response. *Cell* **124**, 803–814 (2006). doi: 10.1016/j.cell.2006.02.008; pmid: 16497589
8. H. Cui, K. Tsuda, J. E. Parker, Effector-triggered immunity: From pathogen perception to robust defense. *Annu. Rev. Plant Biol.* **66**, 487–511 (2015). doi: 10.1146/annurev-arplant-050213-040012; pmid: 25494461
9. E. Lukasik, F. L. Takken, STANDing strong, resistance proteins instigators of plant defence. *Curr. Opin. Plant Biol.* **12**, 427–436 (2009). doi: 10.1016/j.pbi.2009.03.001; pmid: 19394891
10. S. J. Riedl, W. Li, Y. Chao, R. Schwarzenbacher, Y. Shi, Structure of the apoptotic protease-activating factor 1 bound to ADP. *Nature* **434**, 926–933 (2005). doi: 10.1038/nature03465; pmid: 15829969
11. T. F. Reubold, S. Wohlgemuth, S. Eschenburg, Crystal structure of full-length Apaf-1: How the death signal is relayed in the mitochondrial pathway of apoptosis. *Structure* **19**, 1074–1083 (2011). doi: 10.1016/j.str.2011.05.013; pmid: 21827944
12. S. Maekawa, U. Ohto, T. Shibata, K. Miyake, T. Shimizu, Crystal structure of NOD2 and its implications in human disease. *Nat. Commun.* **7**, 11813 (2016). doi: 10.1038/ncomms11813; pmid: 27283905
13. Z. Hu *et al.*, Crystal structure of NLRC4 reveals its autoinhibition mechanism. *Science* **341**, 172–175 (2013). doi: 10.1126/science.1236381; pmid: 23765277
14. W. I. Tameling *et al.*, The tomato R gene products I-2 and MI-1 are functional ATP binding proteins with ATPase activity. *Plant Cell* **14**, 2929–2939 (2002). doi: 10.1105/tpc.005793; pmid: 12417711
15. S. J. Williams *et al.*, An autoactive mutant of the M flax rust resistance protein has a preference for binding ATP, whereas wild-type M protein binds ADP. *Mol. Plant-Microbe Interact.* **24**, 897–906 (2011). doi: 10.1094/MPMI-03-11-0052; pmid: 21539434
16. M. Bernoux *et al.*, Comparative analysis of the flax immune receptors L6 and L7 suggests an equilibrium-based switch activation model. *Plant Cell* **28**, 146–159 (2016). pmid: 26744216
17. M. Zhou *et al.*, Atomic structure of the apoptosome: Mechanism of cytochrome *c*– and dATP-mediated activation of Apaf-1. *Genes Dev.* **29**, 2349–2361 (2015). doi: 10.1101/gad.272278.115; pmid: 26543158
18. Z. Hu *et al.*, Structural and biochemical basis for induced self-propagation of NLRC4. *Science* **350**, 399–404 (2015). doi: 10.1126/science.aac5489; pmid: 26449475
19. L. Zhang *et al.*, Cryo-EM structure of the activated NAIP2-NLRC4 inflammasome reveals nucleated polymerization. *Science* **350**, 404–409 (2015). doi: 10.1126/science.aac5789; pmid: 26449474
20. J. L. Tenthorey *et al.*, The structural basis of flagellin detection by NAIP5: A strategy to limit pathogen immune evasion. *Science* **358**, 888–893 (2017). doi: 10.1126/science.aao1140; pmid: 29146805
21. Z. Hu, J. Chai, Structural mechanisms in NLR inflammasome assembly and signaling. *Curr. Top. Microbiol. Immunol.* **397**, 23–42 (2016). doi: 10.1007/978-3-319-41171-2_2; pmid: 27460803
22. Y. Li *et al.*, Mechanistic insights into caspase-9 activation by the structure of the apoptosome holoenzyme. *Proc. Natl. Acad. Sci. U.S.A.* **114**, 1542–1547 (2017). doi: 10.1073/pnas.1620626114; pmid: 28143931
23. A. Bentham, H. Burdett, P. A. Anderson, S. J. Williams, B. Kobe, Animal NLRs provide structural insights into plant NLR function. *Ann. Bot.* **119**, 827–702 (2017). pmid: 27562749
24. M. R. Swiderski, D. Birker, J. D. Jones, The TIR domain of TIR-NB-LRR resistance proteins is a signaling domain involved in cell death induction. *Mol. Plant-Microbe Interact.* **22**, 157–165 (2009). doi: 10.1094/MPMI-22-2-0157; pmid: 19132868
25. S. M. Collier, L. P. Hamel, P. Moffett, Cell death mediated by the N-terminal domains of a unique and highly conserved class of NB-LRR protein. *Mol. Plant-Microbe Interact.* **24**, 918–931 (2011). doi: 10.1094/MPMI-03-11-0050; pmid: 21501087
26. T. Maekawa *et al.*, Coiled-coil domain-dependent homodimerization of intracellular barley immune receptors defines a minimal functional module for triggering cell death. *Cell Host Microbe* **9**, 187–199 (2011). doi: 10.1016/j.chom.2011.02.008; pmid: 21402358
27. M. Bernoux *et al.*, Structural and functional analysis of a plant resistance protein TIR domain reveals interfaces for self-association, signaling, and autoregulation. *Cell Host Microbe* **9**, 200–211 (2011). doi: 10.1016/j.chom.2011.02.009; pmid: 21402359
28. S. Cesari *et al.*, Cytosolic activation of cell death and stem rust resistance by cereal MLA-family CC-NLR proteins. *Proc. Natl. Acad. Sci. U.S.A.* **113**, 10204–10209 (2016). doi: 10.1073/pnas.1605483113; pmid: 27555587
29. J. D. Lewis, R. Wu, D. S. Guttman, D. Desveaux, Allele-specific virulence attenuation of the *Pseudomonas syringae* HopZ1a type III effector via the *Arabidopsis* ZAR1 resistance protein. *PLOS Genet.* **6**, e1000894 (2010). doi: 10.1371/journal.pgen.1000894; pmid: 20368970
30. A. Schultink, T. Qi, J. Bally, B. Staskawicz, Using forward genetics in *Nicotiana benthamiana* to uncover the immune signaling pathway mediating recognition of the *Xanthomonas perforans* effector XopJ4. *New Phytol.* **221**, 1001–1009 (2019). doi: 10.1111/nph.15411; pmid: 30156705
31. J. D. Lewis *et al.*, The *Arabidopsis* ZED1 pseudokinase is required for ZAR1-mediated immunity induced by the *Pseudomonas syringae* type III effector HopZ1a. *Proc. Natl. Acad. Sci. U.S.A.* **110**, 18722–18727 (2013). doi: 10.1073/pnas.1315520110; pmid: 24170858
32. G. Wang *et al.*, The decoy substrate of a pathogen effector and a pseudokinase specify pathogen-induced modified-self recognition and immunity in plants. *Cell Host Microbe* **18**, 285–295 (2015). doi: 10.1016/j.chom.2015.08.004; pmid: 26355215
33. D. Seto *et al.*, Expanded type III effector recognition by the ZAR1 NLR protein using ZED1-related kinases. *Nat. Plants* **3**, 17027 (2017). doi: 10.1038/nplants.2017.27; pmid: 28288096
34. J. Wang *et al.*, Ligand-triggered allosteric ADP release primes a plant NLR complex. *Science* **364**, eaav5868 (2019).
35. X. Yang *et al.*, Structural basis for specific flagellin recognition by the NLR protein NAIP5. *Cell Res.* **28**, 35–47 (2018). doi: 10.1038/cr.2017.148; pmid: 29182158
36. S. Qi *et al.*, Crystal structure of the *Caenorhabditis elegans* apoptosome reveals an octameric assembly of CED-4. *Cell* **141**, 446–457 (2010). doi: 10.1016/j.cell.2010.03.017; pmid: 20434985
37. X. Jiang, X. Wang, Cytochrome *c* promotes caspase-9 activation by inducing nucleotide binding to Apaf-1. *J. Biol. Chem.* **275**, 31199–31203 (2000). doi: 10.1074/jbc.C000405200; pmid: 10940292
38. P. N. Bryan, J. Orban, Proteins that switch folds. *Curr. Opin. Struct. Biol.* **20**, 482–488 (2010). doi: 10.1016/j.sbi.2010.06.002; pmid: 20591649
39. L. W. Casey *et al.*, The CC domain structure from the wheat stem rust resistance protein Sr33 challenges paradigms for dimerization in plant NLR proteins. *Proc. Natl. Acad. Sci. U.S.A.* **113**, 12856–12861 (2016). doi: 10.1073/pnas.1609922113; pmid: 27791121
40. W. Hao, S. M. Collier, P. Moffett, J. Chai, Structural basis for the interaction between the potato virus X resistance protein (Rx) and its cofactor Ran GTPase-activating protein 2 (RanGAP2). *J. Biol. Chem.* **288**, 35868–35876 (2013). doi: 10.1074/jbc.M113.517417; pmid: 24194517
41. O. Pornillos, B. K. Ganser-Pornillos, M. Yeager, Atomic-level modelling of the HIV capsid. *Nature* **469**, 424–427 (2011). doi: 10.1038/nature09640; pmid: 21248851
42. F. El Kasmi *et al.*, Signaling from the plasma-membrane localized plant immune receptor RPM1 requires self-association of the full-length protein. *Proc. Natl. Acad. Sci. U.S.A.* **114**, E7385–E7394 (2017). doi: 10.1073/pnas.1708288114; pmid: 28808003
43. M. Baudin, J. A. Hassan, K. J. Schreiber, J. D. Lewis, Analysis of the ZAR1 immune complex reveals determinants for immunity and molecular interactions. *Plant Physiol.* **174**, 2038–2053 (2017). doi: 10.1104/pp.17.00441; pmid: 28652264
44. Z. Gao, E. H. Chung, T. K. Eitas, J. L. Dangl, Plant intracellular innate immune receptor Resistance to *Pseudomonas syringae pv. maculicola 1* (RPM1) is activated at, and functions on, the plasma membrane. *Proc. Natl. Acad. Sci. U.S.A.* **108**, 7619–7624 (2011). doi: 10.1073/pnas.1104410108; pmid: 21490299

45. J. M. Elmore, J. Liu, B. Smith, B. Phinney, G. Coaker, Quantitative proteomics reveals dynamic changes in the plasma membrane during *Arabidopsis* immune signaling. *Mol. Cell. Proteomics* **11**, 014555 (2012). doi: 10.1074/mcp.M111.014555; pmid: 22215637
46. D. Qi, B. J. DeYoung, R. W. Innes, Structure-function analysis of the coiled-coil and leucine-rich repeat domains of the RPS5 disease resistance protein. *Plant Physiol.* **158**, 1819–1832 (2012). doi: 10.1104/pp.112.194035; pmid: 22331412
47. T. Chen *et al*., Antiviral resistance protein Tm-2^2 functions on the plasma membrane. *Plant Physiol.* **173**, 2399–2410 (2017). doi: 10.1104/pp.16.01512; pmid: 28258211
48. K. Tanaka, J. M. Caaveiro, K. Morante, J. M. González-Mañas, K. Tsumoto, Structural basis for self-assembly of a cytolytic pore lined by protein and lipid. *Nat. Commun.* **6**, 6337 (2015). doi: 10.1038/ncomms7337; pmid: 25716479
49. M. J. Axtell, B. J. Staskawicz, Initiation of *RPS2*-specified disease resistance in *Arabidopsis* is coupled to the AvrRpt2-directed elimination of RIN4. *Cell* **112**, 369–377 (2003). doi: 10.1016/S0092-8674(03)00036-9; pmid: 12581526
50. D. Mackey, Y. Belkhadir, J. M. Alonso, J. R. Ecker, J. L. Dangl, *Arabidopsis* RIN4 is a target of the type III virulence effector AvrRpt2 and modulates RPS2-mediated resistance. *Cell* **112**, 379–389 (2003). doi: 10.1016/S0092-8674(03)00040-0; pmid: 12581527
51. S. Bieri *et al*., RAR1 positively controls steady state levels of barley MLA resistance proteins and enables sufficient MLA6 accumulation for effective resistance. *Plant Cell* **16**, 3480–3495 (2004). doi: 10.1105/tpc.104.026682; pmid: 15548741
52. Y. Kawano *et al*., Palmitoylation-dependent membrane localization of the rice resistance protein Pit is critical for the activation of the small GTPase OsRac1. *J. Biol. Chem.* **289**, 19079–19088 (2014). doi: 10.1074/jbc.M114.569756; pmid: 24841201
53. I. R. Crute, E. B. Holub, J. J. Burdon, Eds., *The Gene-for-Gene Relationship in Plant-Parasite Interactions*. (CAB International, 1997).
54. S. Engelhardt *et al*., Separable roles of the *Pseudomonas syringae* pv. *phaseolicola* accessory protein HrpZ1 in ion-conducting pore formation and activation of plant immunity. *Plant J.* **57**, 706–717 (2009). doi: 10.1111/j.1365-313X.2008.03723.x; pmid: 18980650
55. D. Pontier, R. Mittler, E. Lam, Mechanism of cell death and disease resistance induction by transgenic expression of bacterio-opsin. *Plant J.* **30**, 499–509 (2002). doi: 10.1046/j.1365-313X.2002.01307.x; pmid: 12047625
56. C. Lacomme, S. Santa Cruz, Bax-induced cell death in tobacco is similar to the hypersensitive response. *Proc. Natl. Acad. Sci. U.S.A.* **96**, 7956–7961 (1999). doi: 10.1073/pnas.96.14.7956; pmid: 10393929
57. J. Ding *et al*., Pore-forming activity and structural autoinhibition of the gasdermin family. *Nature* **535**, 111–116 (2016). doi: 10.1038/nature18590; pmid: 27281216
58. X. Liu *et al*., Inflammasome-activated gasdermin D causes pyroptosis by forming membrane pores. *Nature* **535**, 153–158 (2016). doi: 10.1038/nature18629; pmid: 27383986
59. L. Sborgi *et al*., GSDMD membrane pore formation constitutes the mechanism of pyroptotic cell death. *EMBO J.* **35**, 1766–1778 (2016). doi: 10.15252/embj.201694696; pmid: 27418190
60. Z. Cai *et al*., Plasma membrane translocation of trimerized MLKL protein is required for TNF-induced necroptosis. *Nat. Cell Biol.* **16**, 55–65 (2014). doi: 10.1038/ncb2883; pmid: 24316671
61. X. Chen *et al*., Translocation of mixed lineage kinase domain-like protein to plasma membrane leads to necrotic cell death. *Cell Res.* **24**, 105–121 (2014). doi: 10.1038/cr.2013.171; pmid: 24366341
62. H. Wang *et al*., Mixed lineage kinase domain-like protein MLKL causes necrotic membrane disruption upon phosphorylation by RIP3. *Mol. Cell* **54**, 133–146 (2014). doi: 10.1016/j.molcel.2014.03.003; pmid: 24703947
63. J. P. Erzberger, J. M. Berger, Evolutionary relationships and structural mechanisms of AAA+ proteins. *Annu. Rev. Biophys. Biomol. Struct.* **35**, 93–114 (2006). doi: 10.1146/annurev.biophys.35.040405.101933; pmid: 16689629
64. P. Mestre, D. C. Baulcombe, Elicitor-mediated oligomerization of the tobacco N disease resistance protein. *Plant Cell* **18**, 491–501 (2006). doi: 10.1105/tpc.105.037234; pmid: 16387833
65. K. J. Schreiber, A. Bentham, S. J. Williams, B. Kobe, B. J. Staskawicz, Multiple domain associations within the Arabidopsis immune receptor RPP1 regulate the activation of programmed cell death. *PLOS Pathog.* **12**, e1005769 (2016). doi: 10.1371/journal.ppat.1005769; pmid: 27427964
66. G. J. Rairdan *et al*., The coiled-coil and nucleotide binding domains of the potato Rx disease resistance protein function in pathogen recognition and signaling. *Plant Cell* **20**, 739–751 (2008). doi: 10.1105/tpc.107.056036; pmid: 18344282
67. C. H. Wu *et al*., NLR network mediates immunity to diverse plant pathogens. *Proc. Natl. Acad. Sci. U.S.A.* **114**, 8113–8118 (2017). doi: 10.1073/pnas.1702041114; pmid: 28698366
68. B. Castel *et al*., Diverse NLR immune receptors activate defence via the RPW8-NLR NRG1. *New Phytol.* 10.1111/nph.15659 (2018). pmid: 30582759
69. T. Qi *et al*., NRG1 functions downstream of EDS1 to regulate TIR-NLR-mediated plant immunity in *Nicotiana benthamiana*. *Proc. Natl. Acad. Sci. U.S.A.* **115**, E10979–E10987 (2018). doi: 10.1073/pnas.1814856115; pmid: 30373842
70. Z. Wu *et al*., Differential regulation of TNL-mediated immune signaling by redundant helper CNLs. *New Phytol.* 10.1111/nph.15665 (2018). pmid: 30585636
71. J. R. Peart, P. Mestre, R. Lu, I. Malcuit, D. C. Baulcombe, NRG1, a CC-NB-LRR protein, together with N, a TIR-NB-LRR protein, mediates resistance against tobacco mosaic virus. *Curr. Biol.* **15**, 968–973 (2005). doi: 10.1016/j.cub.2005.04.053; pmid: 15916955
72. V. Bonardi *et al*., Expanded functions for a family of plant intracellular immune receptors beyond specific recognition of pathogen effectors. *Proc. Natl. Acad. Sci. U.S.A.* **108**, 16463–16468 (2011). doi: 10.1073/pnas.1113726108; pmid: 21911370
73. S. Xiao *et al*., Broad-spectrum mildew resistance in *Arabidopsis thaliana* mediated by *RPW8*. *Science* **291**, 118–120 (2001). doi: 10.1126/science.291.5501.118; pmid: 11141561
74. T. Boller, G. Felix, A renaissance of elicitors: Perception of microbe-associated molecular patterns and danger signals by pattern-recognition receptors. *Annu. Rev. Plant Biol.* **60**, 379–406 (2009). doi: 10.1146/annurev.arplant.57.032905.105346; pmid: 19400727
75. M. Toyota *et al*., Glutamate triggers long-distance, calcium-based plant defense signaling. *Science* **361**, 1112–1115 (2018). doi: 10.1126/science.aat7744; pmid: 30213912

ACKNOWLEDGMENTS

We thank J. Lei, X. Li, X. Fan, and N. Liu at Tsinghua University for data collection and P. Schulze-Lefert at the Max Planck Institute for Plant Breeding Research for critical reading of the manuscript. We thank Y. Liu and J. Cao at Tsinghua University for guiding the PM isolation assay. We acknowledge the Tsinghua University Branch of the China National Center for Protein Sciences (Beijing) for providing the cryo-EM facility support and the computational facility support on the cluster of Bio-Computing Platform. **Funding:** This research was funded by the National Natural Science Foundation of China (31421001 to J.C. and 31700660 to Jiz. Wang), the Alexander von Humboldt Foundation (a Humboldt professorship to J.C.), Max Planck-Gesellschaft (a Max Planck fellowship to J.C.), the Strategic Priority Research Program of the Chinese Academy of Sciences (XDB11020200 to J.-M.Z.), the National Key R&D Program of China (grant 2016YFA0501100 to H.-W.W.), the Beijing Municipal Science & Technology Commission (grant Z161100000116034 to H.-W.W.), and the China Postdoctoral Science Foundation (2017T100065 to Jiz. Wang and 2017M620746 to Jia Wang). **Author contributions:** J.C., J.-M.Z., and H.-W.W. conceptualized the project; J.C., J.-M.Z., H.-W.W., Jiz. Wang, M.H., and Jia Wang developed the methodology; Jiz. Wang, M.H., Jia Wang, and J.Q. performed the investigations; Jiz. Wang, M.H., Jia Wang, and G.W. validated the data; J.C., J.-M.Z., H.-W.W., Y.Q., and Z.H. supervised the work; J.C. wrote the original draft of the manuscript; J.C., J.-M.Z., H.-W.W., Jiz. Wang, Jia Wang, and M.H. reviewed and edited the manuscript; and J.C., J.-M.Z., H.-W.W., and Jiz. Wang acquired funding for the project. **Competing interests:** The authors declare no competing interests. **Data and materials availability:** All data needed to replicate the work are present either in the supplementary materials or in the listed Protein Data Bank (PDB) files. For the ZAR1 resistosome and the ZAR1 resistosome with one side enhanced, the atomic coordinates have been deposited in the PDB with accession codes 6J5T and 6J6I, respectively. The EM maps have been deposited in the Electron Microscopy Database with accession codes EMD-0680 and EMD-0688, respectively.

SUPPLEMENTARY MATERIALS

www.sciencemag.org/content/364/6435/eaav5870/suppl/DC1
Materials and Methods
Figs. S1 to S19
Table S1
References (*76*–*91*)
Movie S1

1 October 2018; accepted 13 February 2019
10.1126/science.aav5870

Reconstitution and structure of a plant NLR resistosome conferring immunity

Jizong Wang, Meijuan Hu, Jia Wang, Jinfeng Qi, Zhifu Han, Guoxun Wang, Yijun Qi, Hong-Wei Wang, Jian-Min Zhou and Jijie Chai

Science **364** (6435), eaav5870.
DOI: 10.1126/science.aav5870

The plant resistosome comes into focus

Nucleotide-binding, leucine-rich repeat receptors (NLRs) initiate immune responses when they sense a pathogen-associated effector. In animals, oligomerization of NLRs upon binding their effectors is key to downstream activity, but plant systems differ in many ways and their activation mechanisms have been less clear. In two papers, Wang *et al.* studied the composition and structure of an NLR called ZAR1 in the small mustard plant *Arabidopsis* (see the Perspective by Dangl and Jones). They determined cryo–electron microscopy structures that illustrate differences between inactive and intermediate states. The active, intermediate state of ZAR1 forms a wheel-like pentamer, called the resistosome. In this activated complex, a set of helices come together to form a funnel-shaped structure required for immune responsiveness and association with the plasma membrane.

Science, this issue p. eaav5868, p. eaav5870; see also p. 31